IAI Journals.ASM.org

Structural and Functional Properties of Staphylococcal Superantigen-Like Protein 4

Stefan J. Hermans,[a,c] Heather M. Baker,[b,c] Richard P. Sequeira,[a,c] Ries J. Langley,[a,c] Edward N. Baker,[b,c] and John D. Fraser[a,c]

School of Medical Sciences[a] and Biological Sciences[b] and Maurice Wilkins Centre,[c] University of Auckland, Aukland, New Zealand

Staphylococcus aureus **is a prevalent and significant human pathogen. Among the repertoire of virulence factors produced by this bacterium are the 14 staphylococcal superantigen-like (SSL) proteins. SSL protein 4 (SSL4) is one member of this family and contains a highly conserved carbohydrate binding site also found in SSL2, SSL3, SSL5, SSL6, and SSL11. Recombinant $SSL4_t$, comprising amino acids 109 to 309 of Newman strain SSL4 (SSL4-Newman), has been shown to bind and be internalized by human granulocytes and macrophages in a sialic-acid (Sia)-dependent manner. $SSL4_t$ can compete with itself for cell binding, indicating that binding is target specific. A 2.5-Å-resolution crystal structure of $SSL4_t$ complexed with sialyl Lewis X (sLe^x) [sLe^x-Neu5Acα2-3Galβ1-4(Fucα1-3)GlcNAc] revealed a similar binding site to SSL5 and SSL11. These data, along with data on $SSL4_t$ binding to a glycan array and biosensor analysis of sLe^x and sialyllactosamine (sLacNac) binding are compared with those for SSL11. Although these proteins show great similarity in their carbohydrate binding sites, with a root mean square (RMS) difference between main chain atom positions of only 0.34 Å, these proteins differ in detail in their affinity for sLe^x and sLacNac, as well as their glycan preference. Together with cell binding data, this shows how *S. aureus* produces multiple related proteins that target myeloid cells through specific sialyllactosamine-containing glycoproteins.**

Staphylococcus aureus is the most common cause of hospital-acquired infection (18, 19, 29) and also causes serious acute community-acquired infections in otherwise healthy individuals. *S. aureus* infects almost any tissue in the body and produces an array of cell surface and secreted virulence factors that contribute to its capacity to cause disease (9, 17, 20, 22, 30, 37, 41). Among its repertoire of immune-suppressive virulence proteins are the staphylococcal superantigen (Sag)-like (SSL) proteins, which share structural similarity with the classical superantigens (2, 25).

A total of 11 unique *ssl* genes reside within an almost contiguous region of the staphylococcal genome in a genomic island known as vSaα (24, 28). vSaα is present in all *S. aureus* genomes sequenced thus far and has been hypothesized to play an essential role in the evolution of this microbe as a major human pathogen (3). Despite their structural similarity to superantigens, SSLs do not bind to T-cell receptors or major histocompatibility complex class II molecules and do not stimulate T cells (2). Rather they target components of innate immunity, such as complement, Fc receptors, and myeloid cells. SSL protein 7 (SSL7) is the best characterized of the SSLs and binds complement factor C5 and IgA with high affinity and inhibits the end stage of complement activation and IgA binding to FcαR (27, 36). SSL10 binds to the Fc region of human IgG1 and blocks FcγR-mediated phagocytosis (35).

Unlike SSL7 and SSL10, SSL5 and SSL11 target myeloid cells by binding to cell surface glycoproteins containing the minimal trisaccharide siallylactosamine (sLacNac) (sLacNac-NeuAcα2-3-Galβ1-4-NAGluc). The crystal structures of SSL5 and SSL11 complexed with the blood group antigen sialyl Lewis X (sLe^x) [sLe^x-Neu5Acα2-3Galβ1-4(Fucα1-3)GlcNAc] have revealed a conserved binding site located in the C-terminal β-grasp domain (4, 11). sLe^x is essential to the inflammatory response and is constitutively expressed on granulocytes, regulating selectin-mediated tethering to endothelial cells and extravasation of neutrophils into the tissue to fight infection (32). Both SSL5 and SSL11 bind to neutrophils and inhibit P-selectin-mediated neutrophil rolling at a nanomolar concentration (7, 11). Interestingly SSL5 and SSL11 are rapidly internalized by neutrophils in an energy-dependent fashion, but it remains to be determined which intracellular molecules are targeted once inside the cell (4, 11). Structural modeling of all of the SSLs suggests that carbohydrate binding is shared by a subgroup that includes SSL2, SSL3, SSL4, SSL5, SSL6, and SSL11 (4). Recently it was shown SSL3 binds and inhibits Toll-like receptor 2 (TLR2) activation at the surface of human and murine neutrophils and monocytes in a partially glycan-dependent manner (5).

Here we show that SSL4 also binds to myeloid cells in a glycan-dependent fashion, similar to SSL11, and is rapidly internalized by neutrophils and macrophages and, to a lesser extent, monocytes. The crystal structure of SSL4 complexed with sLe^x reveals the carbohydrate binding site in atomic detail and enables us to explain small but significant differences in binding affinity and specificity compared with SSL11.

MATERIALS AND METHODS

Sequence comparisons were made using ClustalW (10), protein structure figures were prepared using PyMOL (http://www.pymol.org), flow cytometry figures were prepared using FlowJo, and confocal microscopy figures were prepared using FV10-ASW (Olympus).

Production of rSSL4 and mutant SSL4. The gene encoding SSL4 from the published Newman strain (NCBI GeneID no. 5332478) of *S. aureus* (3) was amplified by PCR using the primers SSL4-NWM-Fwd (GCGGATCCACAAAACAAGTACCAACAG) and SSL4-NWM-Rev (CCGGAAG

Received 24 July 2012 Returned for modification 13 August 2012
Accepted 28 August 2012
Published ahead of print 4 September 2012
Editor: R. P. Morrison
Address correspondence to John D. Fraser, jd.fraser@auckland.ac.nz.
Supplemental material for this article may be found at http://iai.asm.org/.

doi:10.1128/IAI.00764-12

CTTTTATTTTATATTCACTTCAATGTTATC). The resulting products were cut using the restriction enzymes BamHI (underlined in the forward primer) and HindIII (underlined in the reverse primer) and cloned into the pET32a.3C vector. This construct comprises amino acids 109 to 309 of SSL4-Newman and is designated $SSL4_t$. The gene encoding SSL11 from the naturally occurring US6610 strain of *S. aureus* had been previously cloned into the pET32a.3c vector by Chung et al. (11). Recombinant $SSL4_t$ and SSL11 ($rSSL4_t$ and rSSL11, respectively) were expressed in *Escherichia coli* AD494 as thioredoxin fusion proteins, as described previously (2, 26). Thioredoxin was cleaved off with 3C protease; $rSSL4_t$ and rSSL11 were further purified using ion-exchange chromatography (MonoS and MonoQ columns; GE Healthcare). Site-directed mutagenesis of $SSL4_t$ by overlap PCR (4, 11) using the primers R182A-Fwd (CAAGAAAATGCC ATGGCAGATGTCATAGATG) and R182A-Rev (CTGCCATGGCATTT TCTTGTAATTTTTTGTGC) was performed to introduce the Arg-182→Ala mutation. The Asn-181→His mutation was introduced using the primers N181H-Fwd (TTACAAGAACATCGCATGGCAGATGTCA TAG) and N181H-Rev (CCATGCGATGTTCTTGTAATTTTTTGTGC AA). The amplified products were cloned into pET32a.3C vector, and the mutations were confirmed by sequencing. The $rSSL4_t$-R182A and $rSSL4_t$-N181H mutant proteins were expressed and purified as for $SSL4_t$. SSL proteins were labeled with one of the amine-reactive dyes Alexa Fluor 488, Alexa Fluor 647 (Invitrogen), or fluorescein isothiocyanate (FITC) (Molecular Probes) as per the manufacturer's instructions.

Crystallization of SSL4 and its complex with sLe^x. $SSL4_t$ crystallization trials were carried out with sitting drops (100 nl protein plus 100 nl precipitant) dispensed by a Cartesian Honeybee nanoliter-dispensing robot (Genomic solutions) using a 480-condition crystallization screen (31) at 18°C. Following optimization, the highest-quality $SSL4_t$ crystals grew in sitting drops of 1 μl $SSL4_t$ (14.5 mg/ml in 20 mM Tris [pH 7.4], 100 mM NaCl) and 1 μl precipitant solution (0.2 M bis-tris-propane [pH 6.5], 21% methyl polyethylene glycol 5000 [MPEG 5000]). Crystallization trials were carried out for $SSL4_t$ complexed with sLe^x (Dextra Laboratories, United Kingdom) as for $SSL4_t$. Following optimization, the highest-quality crystals grew in sitting drops of 1 μl protein solution (13.5 mg/ml $rSSL4_t$, 10 mM sLe^x in 10 mM Tris [pH 7.4], 150 mM NaCl) and 2 μl precipitant solution {0.18 M PIPES [piperazine-*N*,*N*′-bis(2-ethanesulfonic acid)] (pH 6.7), 28% MPEG 5000}. The crystals were mounted in cryoloops, transferred to a cryoprotectant solution that consisted of the precipitant solution plus 20% glycerol for the $SSL4_t$ crystal or 17% glycerol for the $SSL4_t$ sLe^x complex crystal and flash-cooled by being plunged into liquid nitrogen.

Data collection and processing. X-ray diffraction data for both crystals were collected at 100 K using CuKα radiation (λ = 1.5418 Å) from a Rigaku Micromax-007 HF rotating anode generator equipped with Osmic mirrors, an Oxford cryostream, and a Mar345 imaging plate system. $SSL4_t$ crystal data were processed with MOSFLM and scaled with SCALA from the CCP4 suite (12). The data set was more than 99% complete to a 1.7-Å resolution with a space group of C2. $SSL4_t$ and sLe^x complex data were integrated using XDS (23) and scaled with SCALA. The data set was more than 99% complete to a 2.5-Å resolution with a space group of I222.

Structure determination and refinement. The $SSL4_t$ structure was solved by molecular replacement using PHASER (39) with the structures of SSL5 (Protein Data Bank [PDB; http://www.rcsb.org] ID no. 2Z8L) (2) and SSL11 (PDB ID no. 2RDG) (11) as the search models. The molecular replacement phases were then used with PHENIX (1) to build a contiguous model. This structure was refined through cycles of manual model building using COOT (15) and refinement using REFMAC5 (33). Water molecules were included in the model if they had good spherical density, reasonable B-factors, and favorable hydrogen bonding contacts. Other solvent species were identified from their densities and environment. The structure was validated using MOLPROBITY (14), and the refinement statistics are shown in Table 1. The structure of $SSL4_t$ in complex with sLe^x was solved by molecular replacement using PHASER (39) with the $SSL4_t$ structure as a search model. This structure was refined as for the native $SSL4_t$ structure. Well-defined density was immediately apparent for the complete sLe^x molecule; however, this was not modeled until the protein structure was nearing completion. A restraint library for sLe^x was developed through the program SKETCHER of the CCP4 suite (12). Water molecules and other solvent species were added as described above, and the refinement statistics are shown in Table 1.

TABLE 1 Data collection and refinement statistics parameters

Parameter	Value(s) for[a]: SSL4	Value(s) for[a]: sLe^x complex
Crystal data		
Space group	C2	I222
Cell		
Axial lengths (Å)	96.1, 81.2, 57.3	61.9, 78.9, 97.7
Angles (°)	90.00, 105.45, 90.00	90.00, 90.00, 90.00
Data collection		
Resolution range (Å)	27.62–1.70 (1.79–1.70)	24.42–2.50 (2.64–2.5)
Data collection temp (K)	113	113
No. of unique reflections	46,435	8,563
Completeness (%)	99.7 (99.3)	99.9 (100.00)
Mosaicity (°)	1.02	0.214
R_{merge} (%)	0.058 (0.698)	16.9 (74.7)
I/σ^a	17.4 (2.4)	12.0 (3.1)
Refinement		
Resolution range (Å)	27.62–1.70	24.42–2.50
R/R_{free}	0.2086/0.2614	0.1847/0.2543
Mean B-value (Å^2)	29.7	25.6
RMSD from standard values		
Bond lengths (Å)	0.025	0.017
Bond angles (°)	2.1	1.8
Ramachandran plot		
% of residues in favored regions	97.1	95.3
Outliers	None	None

[a] Throughout, values in parentheses are for the outermost resolution shell.

SSL4 affinity for sLe^x by surface plasmon resonance (SPR). For surface plasmon resonance (SPR), SLe^x-bovine serum albumin (BSA) and sLacNac-BSA (Dextra Laboratories, United Kingdom) were coupled by carbodiimide chemistry to a CM5 biosensor chip surface using a Biacore T200 (GE Healthcare Biacore, Australia) as per the manufacturer's instructions. Coupling was typically 100 to 200 response units (RU). $rSSL4_t$, rSSL11, $rSSL4_t$-N181H, and $rSSL4_t$-R182A were freshly purified by gel filtration chromatography (Superdex; GE Healthcare); the trailing edges of the peaks were used as the analytes (8 μM to 6.125 nM) in HBS-EP+ (0.01 M HEPES [pH 7.4], 0.15 M NaCl, 3 mM EDTA, 0.05% surfactant P20; GE Healthcare) and were passed over the immobilized ligand at 30 μl/min. The response at equilibrium (R_{eq}) was measured as the binding response plateau at 6 min. Equilibrium binding data were fitted to a single-binding-site model using the Biacore T200 evaluation software: $R_{eq}/B_{max} = ([rSSL4_t])/(K_D + [rSSL4_t])$, where R_{eq} is the plateau binding response, B_{max} is the maximal bound analyte at calculated saturation, R_{eq}/B_{max} is the fraction of immobilized ligand bound, and K_D is the affinity constant at equilibrium.

SSL4 glycan binding specificity by glycomics array. Purified FITC-$rSSL4_t$ was submitted to the Centre for Functional Glycomics (http:

//www.functionalglycomics.org; Scripps Research Institute, San Diego, CA). Binding was analyzed at 100 μg/ml to 320 glycans arrayed on a glass slide. Relative binding was measured as relative fluorescent units (RFU). The data from the glycomics array are available in the supplemental material.

SSL4 binding cell populations by flow cytometry. Human leukocytes were purified from blood collected in sodium heparin-containing Vacuette tubes (Griener Bio One). Five milliliters of concentrated erythrocyte lysis buffer (100 mM $KHCO_3$, 9% [wt/vol] NH_4Cl, 1 mM EDTA) was added to 40 ml H_2O and warmed to 20°C. Five milliliters of fresh human blood was added, and the mixture was incubated with constant rotation until the erythrocytes were lysed, before centrifugation. The cells were washed and resuspended in phosphate-buffered saline (PBS)–0.5% bovine serum albumin (BSA) at 1×10^6 cells/ml. A 0.5 μM concentration of FITC-labeled $rSSL4_t$ and 5 μl/ml CD14-phycoerythrin (PE) conjugate (M5E2-PE; BD Pharmingen), CD3-PE, CD10-PE, or CD19-PE (SN5c-PE, MEM-57-PE, and LT19-PE, respectively; Serotec) were added to the cells for 30 min before they were washed, resuspended in PBS–0.5% BSA, and analyzed on a BD LSR II flow cytometer. Neutrophils were purified from blood collected in potassium EDTA-containing Vacutainer tubes (BD Biosciences). Five milliliters of blood was layered over 2.5 ml of Histopaque 1077 (Sigma), which was layered over 2.5 ml of Histopaque 1119 (Sigma) and then centrifuged. The interface was collected, contaminating erythrocytes were lysed by hypotonic saline lysis, and the neutrophils were resuspended in PBS–0.5% BSA at 1×10^6 cells/ml. A 0.5 μM concentration of FITC-labeled $rSSL4_t$ or $rSSL4_t$-R182A was added to the neutrophils for 30 min before they were washed, resuspended in PBS–0.5% BSA, and analyzed on a BD LSR II flow cytometer. For neuraminidase treatment, neutrophils were washed and resuspended at 1×10^7 cells/ml in 150 mM NaCl–5 mM $CaCl_2$ (pH 6.0) and then incubated with 25 U/ml neuraminidase (New England BioLabs) for 1 h at 37°C in 5% CO_2. For complementary binding studies, 0.01 μM Alexa Fluor 488-labeled $rSSL4_t$ and rSSL11 were added to neutrophils with 0.1 μM $rSSL4_t$, rSSL11, or $rSSL4_t$-N181H for 30 min before being washed, resuspended in PBS–0.5% BSA, and analyzed on a BD LSR II flow cytometer.

Cell staining of SSL4 by confocal microscopy. Freshly isolated neutrophils were suspended at 1×10^6 cells/ml and allowed to adhere to a poly-D-lysine-coated 2.3-cm glass plate (World Precision Instruments) in Dulbecco's PBS without Ca^{2+} and Mg^{2+} (Sigma) for 30 min. Monocyte-derived macrophages were prepared as described previously (13). In short, human peripheral blood mononuclear cells (PBMCs) were collected by Histopaque density centrifugation as for neutrophils. Blood for human serum was collected in a serum nongel with a silica Vacutainer tube (BD Biosciences), kept at 20°C for 30 min to clot, and centrifuged. PBMCs at 1×10^6 cells/ml were plated onto a poly-D-lysine-coated 2.3-cm glass plate in RPMI 1640 medium with L-glutamine and sodium bicarbonate (Gibco) containing 10% human serum and incubated at 37°C and 5% CO_2. After 24 h, nonadherent cells were removed and adherent cells were cultured in RPMI with 10% heat-treated fetal bovine serum (FBS) (Invitrogen) at 37°C and 5% CO_2 for 14 days. To prepare primary monocytes, PBMCs at 2×10^6 cells/ml were plated onto a plastic 2.3-cm plate in RPMI 1640 medium with L-glutamine and sodium bicarbonate (Gibco) containing 10% heat-treated FBS (Invitrogen) and incubated at 37°C and 5% CO_2 for 1 h. Selection was by plastic adhesion, and nonadherent cells were removed through PBS washing. Cell-coated plates were washed and incubated with 0.2 μM Alexa Fluor 647 (Invitrogen)-labeled $rSSL4_t$ and 0.2 μM Alexa Fluor 488 (Invitrogen)-labeled rSSL11 in Dulbecco's PBS with Ca^{2+} and Mg^{2+} (Sigma) for 30 min at 37°C or 4°C. The cells were washed with Dulbecco's PBS without Ca^{2+} and Mg^{2+} and visualized using an Olympus FV1000 confocal laser scanning microscope.

Protein structure accession numbers. The atomic coordinates and structure factors for both $SSL4_t$ and $SSL4_t$ complexed with sLe^x have been deposited in the PDB under code no. 4dXF and 4DXG, respectively.

RESULTS

SSL4 was cloned and expressed as a construct that extended from the beginning of the conserved oligosaccharide/oligonucleotide binding (OB)-fold domain and β-grasp domain shared with all SSLs. This removed a variable N-terminal region predicted to have low complexity. When expressed as a full-length peptide, it was observed that this protein degraded to a stable form of identical molecular weight to $SSL4_t$. Additionally a crystal structure of this full-length protein showed there was no electron density for the additional amino acids at the N terminus, which were therefore assumed to be disordered (data not shown). This study has focused on the carbohydrate specificity of the SSLs, which is associated with the conserved glycan binding site in the β-grasp domain of the protein. Therefore, it was decided to clone and express SSL4 without this N-terminal sequence. This does not exclude this region from being of functional significance, where it may augment the cellular effect of this protein.

Comparison of 12 published $SSL4_t$ sequences identified 4 alleles. A sequence alignment of the Newman (identical to MW2, USA300 TCH1516, USA300 FPR3757, NCT88325, and MSSA476), N315 (identical to Mu3, JH1, and JH9), COL, and MRSA252 $SSL4_t$ alleles revealed sequence variation of up to 25% (Fig. 1a). This is primarily attributable to the MRSA252 allele, which displays 23 to 25% sequence variation with the other identified alleles. Sequence variation between the remaining alleles is no more than 8%. Previous amino acid sequence alignments of SSL2, SSL3, SSL4, SSL5, SSL6, and SSL11 from the MW2 *S. aureus* strain revealed remarkable conservation in the sLe^x binding region (4), with 12 of the 17 residues between positions 169 and 185 (SSL4 numbering) being identical in all six SSLs. This is in contrast to the modest similarity seen in the rest of the sequences. An alignment of $SSL4_t$, SSL5, and SSL11 highlights this (Fig. 1b), with only 34% overall sequence identity shared between $SSL4_t$ and SSL5 and 36% identity shared between $SSL4_t$ and SSL11.

The crystal structure of $SSL4_t$ was solved by molecular replacement using the structures of SSL5 and SSL11 as search models. The structure was refined to a resolution of 1.7 Å, with excellent geometry and an *R* value of 20.86% (R_{free}, 26.14%) (Table 1). The final structure contains two $SSL4_t$ chains, residues 7 to 200 in molecule A, residues 11 to 200 in molecule B, 316 water molecules, 1 glycerol molecule, and 4 chloride ions. $SSL4_t$ shows the same characteristic two-domain fold as other superantigens (Sags) and SSLs. The N-terminal domain (residues 1 to 100) forms an OB-fold domain, a five-stranded β-barrel structure comprising β-strands β1 to β5. The C-terminal domain (residues 101 to 200) forms a β-grasp fold in which a central helix (α4) rests against a mixed β-sheet formed from β-strands: β7-β6-β12-β9-β10.

The crystal structure of $SSL4_t$ in complex with sLe^x was then solved by molecular replacement using the high-resolution $SSL4_t$ structure as a model. The structure was refined to a resolution of 2.5 Å, with excellent geometry and an *R* value of 18.47% (R_{free}, 25.43%) (Table 1). The final structure contained one chain of SSL4 from residues 7 to 200, 1 sLe^x molecule, 1 PIPES molecule, 2 chloride ions, and 62 water molecules (Fig. 2a).

Dimers of $SSL4_t$ were formed in both crystal structures as a result of crystal packing. The β7 strands from adjacent symmetry-related molecules aligned in antiparallel fashion, creating a 10-stranded β-sheet between the C-terminal domains of both molecules. The same interaction is seen in all crystal forms of SSL5 and SSL11, indicating that this form of association is of possible func-

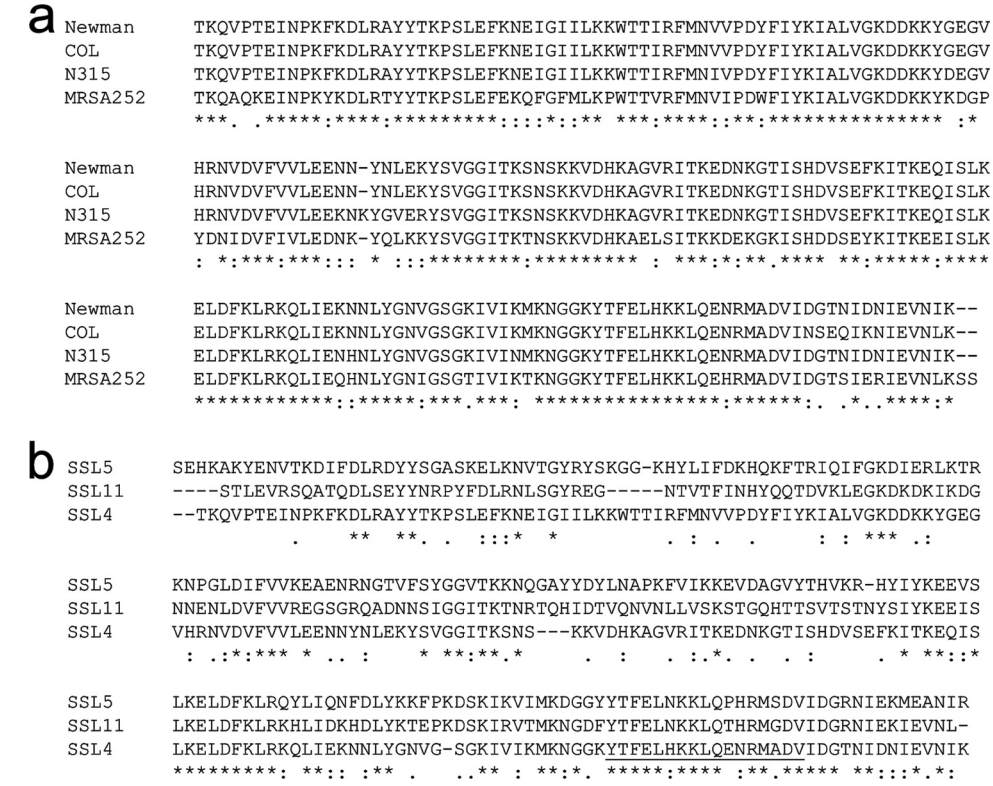

FIG 1 Sequence alignments of $SSL4_t$ alleles and $SSL4_t$, SSL5, and SSL11. (a) Amino acid alignment of known $SSL4_t$ allele variants. Identity (*), strong similarity (:), and weak similarity (.) are indicated. (b) Amino acid alignment of $SSL4_t$ from *S. aureus* strain Newman, SSL5 from strain GL10, and SSL11 from strain US6610. The 17-amino-acid binding site is underlined, and sequence similarity is labeled as described above.

tional significance—for example, at the target cell surface where the proteins could be concentrated. Isothermal titration calorimetry was used to test dimer formation of $SSL4_t$ in solution. $SSL4_t$ was shown not to form dimers at high concentrations in solution (data not shown).

In its complex with $SSL4_t$, sLe^x occupies the same V-shaped loop between strand β10 and a distorted 3_{10} helix, as seen in both SSL5 and SSL11 (Fig. 2b). Comparisons of the RMSDs between main chain atom positions in the 17-residue binding sites and the entire protein chains when aligned reveal the remarkable conservation of the binding loop between these proteins. These are 0.34 Å and 6.31 Å, respectively, between $SSL4_t$ and SSL11 and 0.35 Å and 6.10 Å, respectively, between $SSL4_t$ and SSL5. Key residues of $SSL4_t$ that interact with the sLe^x molecule are Lys-169, Thr-171, and Glu-173 from the β10 strand, Lys-176 from the top of the V-shaped loop, and Gln-179, Asn-181, Arg-182, and Asp-185 from the descending α-helix. $SSL4_t$ makes 14 direct hydrogen bonds with the sLe^x molecule; the majority of these interactions occur with the Sia and galactose (Gal) units of the tetrasaccharide and are identical to those made by SSL5 and SSL11. Differences between the binding sites of $SSL4_t$, SSL5, and SSL11 are seen in the *N*-acetylglucosamine (NAG) and fucose (Fuc) interactions (Fig. 2c). Asn-181 of $SSL4_t$ makes a direct hydrogen bond with O5 of NAG, which allows the conserved Glu-173, Lys-176, and Gln-179 residues of $SSL4_t$ to make four additional hydrogen bonds with the Fuc residue. Asn-181 is replaced in SSL11 by His-178 which, due the longer side chain, forms a direct hydrogen bond with the O6 of NAG and also causes the NAG and Fuc residues to be held 2 to 3 Å further out of the binding pocket in SSL11. This prevents any hydrogen bonding between Lys-173 and Gln-176 of SSL11 and the Fuc of sLe^x. The two available crystal structures of SSL5 and sLe^x show that His-185, equivalent to Asn-181 in $SSL4_t$ and His-178 in SSL11, can have two positions. In position 1, it forms a hydrogen bond with the O6 of NAG and pushes the NAG and Fuc residues out of the binding pocket as for SSL11. In position 2, however, the His flips away, allowing the NAG and Fuc residues to move in closer, just as in $SSL4_t$ (Fig. 2c).

SPR was used to calculate and compare the affinities of SSL4 and SSL11 for the blood group antigen sLe^x and the carbohydrate sLacNac, a subcomponent of sLe^x lacking the terminal fucose. The sLe^x and sLacNac carbohydrates were immobilized onto a chip surface, and highly purified recombinant $SSL4_t$ and SSL11 were then used as soluble analyte. An initial $SSL4_t$ concentration series revealed more than one binding species affecting the binding and dissociation kinetics (data not shown), suggesting the presence of protein aggregates as seen by Chung et al. for SSL11 (11). $SSL4_t$ and SSL11 were further purified by size exclusion chromatography on a Sephadex 10/200 GL fast protein liquid chromatography (FPLC) (GE) column, and fractions from the trailing edge of the protein peaks, presumed to be dominantly monomeric protein in solution, were then analyzed immediately and separately for sLe^x and sLacNac binding. Equilibrium binding curves were obtained from the trailing edge of both $SSL4_t$ and SSL11 binding sLe^x and sLacNac (Fig. 3a, b, e, and f). The equilibrium dissociation constants (K_D) of $SSL4_t$ binding sLe^x and sLacNac were calculated to be 87.0 ± 4.5 nM and 471.7 ± 18.7 nM, respectively, compared

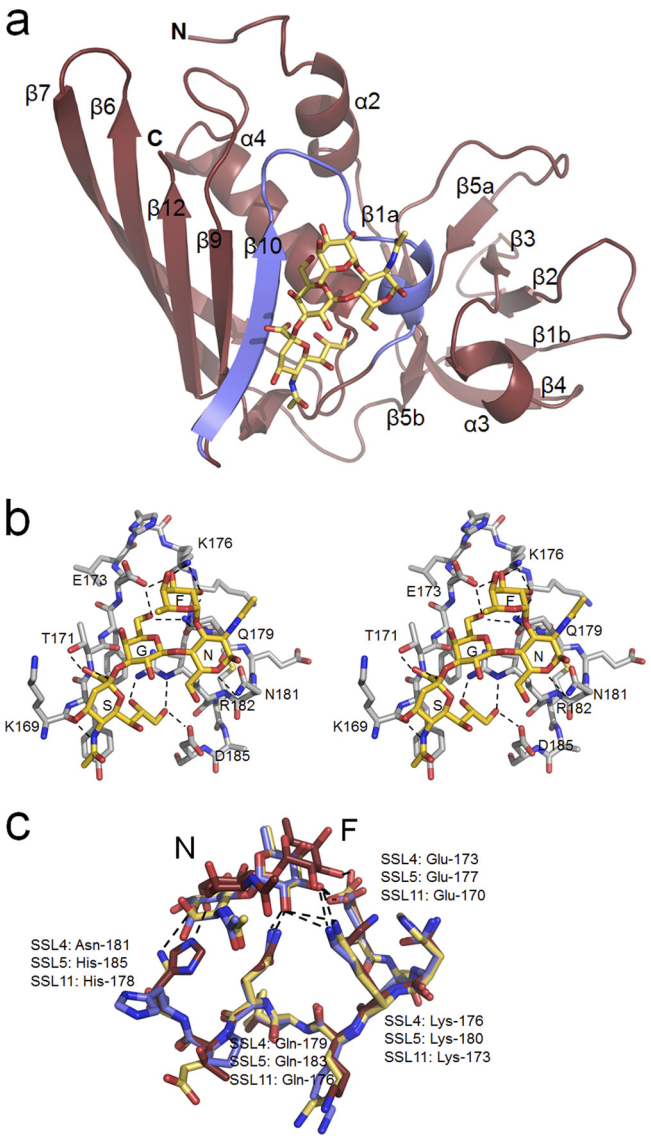

FIG 2 Structure of the $SSL4_t$-sLe^x complex. (a) Ribbon diagram showing the $SSL4_t$-sLe^x complex with secondary structure elements labeled according to standard Sag nomenclature. The N-terminal OB-fold domain is on the right, with the C-terminal β-grasp domain on the left. The bound sLe^x is shown as sticks and sits in a surface depression made by a V-shaped loop between strand β10 and a deformed 3_{10} helix (blue). (b) Stereo view of the sLe^x binding site of $SSL4_t$. sLe^x atoms are colored gold and $SSL4_t$ atoms silver, with element coloring. Hydrogen bonds between sLe^x and protein atoms are shown by dashed lines. sLe^x residues are labeled S (Sia), G (Gal), N (NAG), and F (Fuc), and $SSL4_t$ residues that form direct hydrogen bonds to sLe^x are labeled. (c) Overlay of the interaction between NAG (N) and Fuc (F) of sLe^x and Glu-173, Lys-176, Gln-179, and Asn-181 of $SSL4_t$ (yellow), Glu-170, Lys-173, Gln-176, and His-178 of SSL11 (red), and Glu-177, Lys-180, Gln-183, and His-185 of SSL5 (blue).

with the values 2.32 ± 0.20 μM and 2.43 ± 0.02 μM, respectively, for the same carbohydrates bound by SSL11.

It was hypothesized from the crystal structures of these proteins complexed with sLe^x that the Asn-181 residue of $SSL4_t$ may be responsible for this higher affinity for sLe^x over SSL11. This was tested by mutagenesis; the Asn-181 residue of $SSL4_t$ was mutated to His, the equivalent residue in SSL11. The affinity of the $SSL4_t$-N181H mutant for sLe^x was, however, similar to that of $SSL4_t$, with a calculated K_D of 90.8 ± 6.4 nM. Unlike $SSL4_t$, but identical to SSL11, the dissociation constant of this mutant for sLacNac was very similar to that of sLe^x, with a calculated K_D of 119.1 ± 10.3 nM. The $SSL4_t$ structure also showed that Arg-182 formed the floor of the carbohydrate binding pocket, analogous to Arg-186 in SSL5 and Arg-179 in SSL11. This was confirmed by mutagenesis, with $SSL4_t$-R182A displaying no detectable binding to sLe^x (see the supplemental material). Modeling indicated that the Asn-181→His and Arg-182→Ala mutations should have no effect on the folding or stability of the $SSL4_t$ molecule. Recombinant $SSL4_t$-N181H and $SSL4_t$-R182A were expressed and purified at similar levels in *E. coli* to the parental protein.

SSL4 was tested for binding against 320 different glycans, using a microarray format provided by the Consortium for Functional Glycomics. Glycans were attached through spacer groups SP0 and SP8 to SP21. $SSL4_t$ was tested at 100 μg/ml, and the results for the 10 strongest glycans are presented in Table 2. The core ligand for $SSL4_t$, present in almost all of the top-scoring glycans, was 3′-sLacNac, which was itself represented at position 9 on Table 2. As mentioned earlier, sLacNac is a subcomponent of sLe^x, which is represented in row 3 in Table 2. Like SSL11 (11), $SSL4_t$ does not bind sLacNac, with a β1-3 linkage between the Gal and NAG residues highlighting its preference for this ligand. However, whereas SSL11 does not bind to very similar glycans such as sGal (Neu5Acα2-3Galβ) and sialyllactose (Neu5Acα2-3Galβ1-4Glcβ), $SSL4_t$ displayed moderate binding (Table 2).

FITC-labeled $SSL4_t$ bound strongly to human monocytes (CD14) and neutrophils (CD10) and weakly to T lymphocytes. No binding was observed to B lymphocytes (Fig. 4a). This binding specificity was consistent with multiple individual blood samples tested and was similar in profile to the cell specificity of SSL11 (11). $SSL4_t$ binding was substantially reduced on granulocytes pretreated with 25 U/ml neuraminidase (Fig. 4b), and the $SSL4_t$-R182A mutant displayed no detectable binding to human granulocytes (Fig. 4c). Together, these data indicate that this interaction is carbohydrate dependent. To determine whether SSL4 and SSL11 compete for the same glycosylated targets, complementary binding studies were performed with a low concentration of either fluorescent $SSL4_t$ or SSL11 (0.01 μM) mixed with a 10-fold excess (0.1 μM) of the unlabeled protein. $SSL4_t$ competed effectively and was saturable with itself, suggesting that the majority of binding was to specific surface receptor(s) (Fig. 4d). Excess unlabeled SSL11 had no effect on $SSL4_t$-488 binding (Fig. 4d), indicating that despite a shared affinity for sialylated glycoproteins, the target molecules bound by SSL4 and SSL11 are likely not to be identical. This is consistent with the binding preference differences observed in the glycomics array data. The unlabeled $SSL4_t$-N181H mutant competed effectively with $SSL4_t$-488 to a similar degree as unlabeled $SSL4_t$. Competition using unlabeled SSL11, $SSL4_t$, and $SSL4_t$-N181H with SSL11-488 showed no change in SSL11-488 binding (Fig. 4e), indicating a wider binding specificity from this SSL.

SSL11 is rapidly internalized by human granulocytes in an energy-dependent manner (11). To determine the fate of SSL4, $SSL4_t$ was labeled with Alexa Fluor 647, incubated with human granulocytes at 37°C or 4°C, and monitored by live-cell confocal microscopy. $SSL4_t$ was rapidly internalized by human neutrophils into sharply distinct vesicles at 37°C, whereas at 4°C, it remained surface bound (Fig. 5). We observed that at 4°C, neutrophils ap-

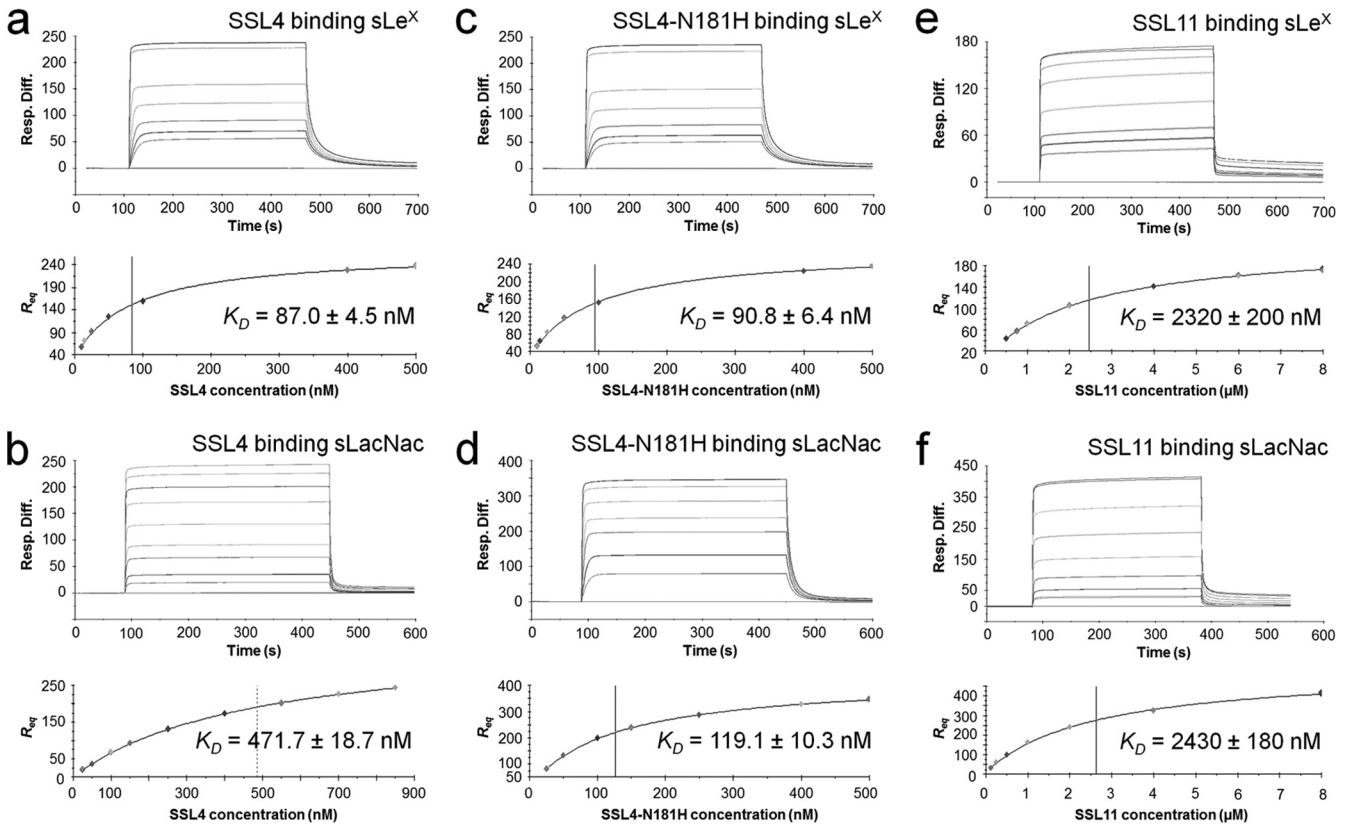

FIG 3 Quantitative measure of $SSL4_t$, $SSL4_t$-N181H, and SSL11 binding to sLe^x and sLacNac. Binding responses (Resp.) at equilibrium (R_{eq}) are shown against the concentration and fitted to a steady-state affinity binding model to calculate an equilibrium affinity constant (K_D). (a) sLe^x sensor chip binding and equilibrium binding analysis of 6.125 to 500 nM $SSL4_t$ in duplicate. The K_D was calculated to be 87.0 ± 4.5 nM. (b) sLacNac sensor chip binding and equilibrium binding analysis of 25 to 850 nM $SSL4_t$ in duplicate. The K_D was calculated to be 471.7 ± 18.7 nM. (c) sLe^x sensor chip binding and equilibrium binding analysis of 6.125 to 500 nM $SSL4_t$-N181H in duplicate. The K_D was calculated to be 90.8 ± 6.4 nM. (d) sLacNac sensor chip binding and equilibrium binding analysis of 25 to 500 nM $SSL4_t$-N181H in duplicate. The K_D was calculated to be 119.1 ± 10.3 nM. (e) sLe^x sensor chip binding and equilibrium binding analysis of 0.5 to 8 μM SSL11 in duplicate. The K_D was calculated to be 2.32 ± 0.20 μM. (f) sLacNac sensor chip binding and equilibrium binding analysis of 0.125 to 8 μM SSL11 in duplicate. The K_D was calculated to be 2.43 ± 0.02 μM. The plots shown are representative of two independent experiments, R_{max} and χ^2 values can be found in Table S1 in the supplemental material.

pear spherical, while at 37°C, they appear to flatten and become amorphous in shape. This is independent of SSL4 binding as we observed these differences in neutrophil morphology in the absence of SSL4 (data not shown). $SSL4_t$ also binds human monocytes, and staining of these cells revealed moderate internalization into vesicles at 37°C but not at 4°C (Fig. 5). Unlike neutrophils, a significant amount of cell-bound $SSL4_t$ appeared to remain at the cell surface; internalization is not as complete in these cells. $SSL4_t$

TABLE 2 SSL4 glycomics array results[a]

Glycan name	Avg no. of RFU	SD
Neu5Acα2-3Galβ1-4(Fucα1-3)GlcNAcβ1-3Galβ1-4GlcNAcβ-Sp8	10,246	1,636
Neu5Acα2-3Galβ1-4(Fucα1-3)GlcNAcβ1-3Galβ1-4(Fucα1-3)GlcNAcβ1-3Galβ1-4(Fucα1-3)GlcNAcβ–Sp0	7,555	449
Neu5Acα2-3Galβ1-4(Fucα1-3)GlcNAcβ–Sp8 (sLe^x)	6,916	2,675
Neu5Acα2-3Galβ1-4GlcNAcβ1-3Galβ1-4GlcNAcβ1-3Galβ1-4GlcNAcβ–Sp0	4,871	967
Neu5Acα2-3Galβ1-4[6OSO3]GlcNAcβ-Sp8	4,717	305
Neu5Acα2-3Galβ1-4(Fucα1-3)GlcNAcβ1-3Galβ-Sp8	4,496	405
Neu5Gca2-3Galβ1-4(Fucα1-3)GlcNAcβ-Sp0	4,444	900
Neu5Acα2-3Galβ1-4GlcNAcβ1-2Manα1-3(Neu5Acα2-3Galβ1-4GlcNAcβ1-2Manα1-6)Manβ1-4GlcNAcβ1-4GlcNAcβ-Sp12	4,253	297
Neu5Acα2-3Galβ1-4GlcNAcβ–Sp8 (sLacNac)	3,774	215
Galβ1-3(Neu5Acα2-3Galβ1-4(Fucα1-3)GlcNAcβ1-6)GalNAc–Sp14	3,525	495
Neu5Acα2-3Galβ1-3GlcNAcβ–Sp8	307	87
Neu5Acα2-3Galβ-Sp8 (sGal)	2,327	172
Neu5Acα2-3Galβ1-4Glcβ–Sp0 (sLac)	517	97
Neu5Acα2-3Galβ1-4Glcβ–Sp8 (sLac)	1,627	167

[a] The 10 strongest glycans are presented in descending order of fluorescence in the top portion of the table.

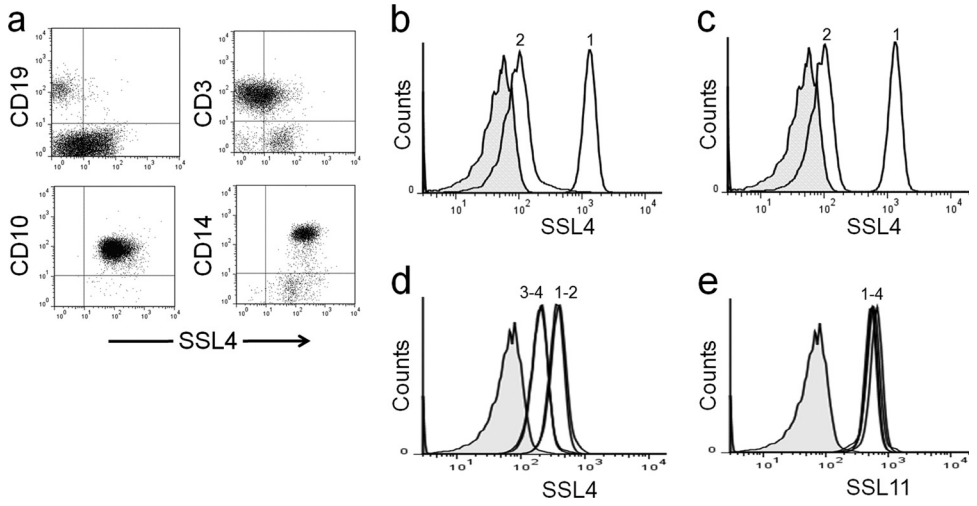

FIG 4 Sialic-acid-dependent binding of $SSL4_t$ to human myeloid cells. (a) Human leukocytes double stained with $rSSL4_t$-FITC (*x* axis) and PE-conjugated antibodies specific to monocytes (CD14), neutrophils (CD10), B lymphocytes (CD19), and T lymphocytes (CD3). (b) Binding of 0.1 μM $SSL4_t$-FITC to human granulocytes untreated (peak 1) or pretreated (peak 2) with neuraminidase. (c) Human granulocytes stained with 0.1 μM $SSL4_t$-FITC (peak 1) or 0.4 μM $SSL4_t$-R182A-FITC (peak 2). (d) Human granulocytes stained with 0.01 μM $SSL4_t$-488 (peak 1) plus 10-fold (0.1 μM) excess of either unlabeled SSL11 (peak 2), unlabeled $SSL4_t$ (peak 3), or unlabeled $SSL4_t$-N181H (peak 4). (e) Human granulocytes stained with 0.01 μM SSL11-488 (peak 1) plus 10-fold (0.1 μM) excess of unlabeled SSL11 (peak 2), unlabeled $SSL4_t$ (peak 3), or unlabeled $SSL4_t$-N181H (peak 4).

was also rapidly internalized into activated human macrophages at 37°C but not at 4°C (Fig. 5). These data reveal $SSL4_t$ binding and complete internalization into neutrophils and macrophages, but only binding and moderate internalization by monocytes. The fluorescent staining pattern of neutrophils and monocytes showed strong intracellular punctate staining, suggesting concentration into vesicles. Macrophages displayed a more diffuse intracellular staining pattern similar to cytoskeletal staining. To confirm that SSL4 and SSL11 were internalized to the same intracellular compartment, neutrophils, monocytes, and macro-

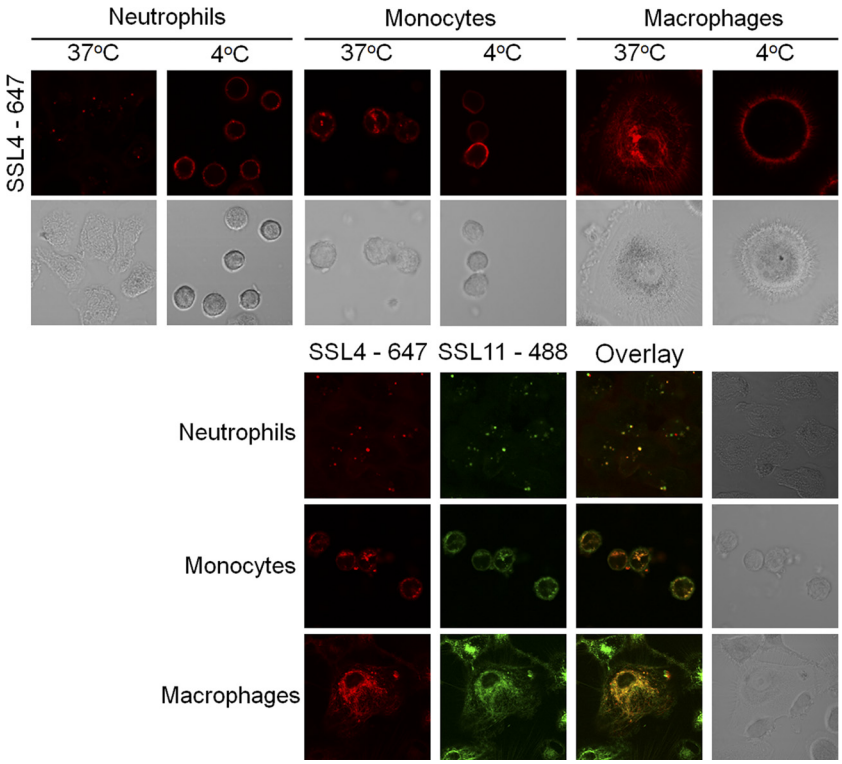

FIG 5 Binding and internalization of $SSL4_t$-647 into neutrophils, monocytes, and macrophages. Cells were incubated with 0.2 μM $SSL4_t$-647 and examined at either 4°C or after cells had been warmed to 37°C. In the lower panel, human neutrophils, monocytes, and macrophages were incubated with 0.2 μM both SSL11-488 and $SSL4_t$-647, and the cells were warmed to 37°C for 30 min. Two color channels were overlaid to identify coincident fluorescence (yellow).

phages were stained with both $SSL4_t$-647 (red) and SSL11-488 (green) at 37°C. Two-color overlay (yellow) confirmed that they both trafficked to the same intracellular location (Fig. 5).

DISCUSSION

The staphylococcal superantigens (Sags) form a family of structurally and functionally related proteins, of which 23 serologically distinct molecules have been described (25, 42). Despite their common structure, Sags utilize a remarkable range of binding properties to carry out their role in stimulating T cells through cross-linking major histocompatibility complex II with the T-cell receptor (34). The SSLs have emerged as a family of structurally related molecules that carry out an entirely different function; these molecules target multiple components of the innate immune response through a variety of structural mechanisms (4, 11, 27). This highlights how *S. aureus* has come to use the simple two-domain fold of the Sags as an adaptable framework in which to generate a plethora of virulence factors that target both the adaptive and innate immune responses.

Both SSL5 and SSL11 have been shown to bind sialated glycans through a conserved binding site in the C-terminal β-grasp domain that is present in several SSLs (4, 11). Here we show that SSL4, a member of this subfamily, binds to sLe^x in an almost identical fashion. The key amino acid residues that interact directly with sLe^x are almost entirely conserved between SSL5, SSL11, and SSL4. Despite this, $SSL4_t$ displays a much higher affinity than SSL11 for sLe^x (K_D = 87.0 nM compared with 2.32 μM), in quantitative binding studies. This is largely due to the substitution for Asn-181 in $SSL4_t$ by His-178 in SSL11, which holds the NAG and Fuc residues 2 to 3 Å further out of the binding pocket compared to SSL4, resulting in three fewer direct hydrogen bonds made between the protein and ligand. Mutation of the equivalent residue of $SSL4_t$, Asn-181, to histidine had little effect on the affinity for sLe^x (K_D = 90.8 nM). We hypothesize that this is because His-181 of $SSL4_t$-N181H can flip out, as seen in SSL5, allowing NAG and Fuc to bind closer to the binding site; although one hydrogen bond to NAG is lost by this, the three additional hydrogen bonds made to Fuc remain. In SSL11, the His-178 cannot flip away as it is held in place by a water-mediated hydrogen bond with the preceding Thr-177. This hydrogen bond could not occur in SSL4 and SSL5, in which the residues equivalent to Thr-177 are glutamic acid and proline, respectively. We further predict SSLs with an asparagine or aspartic acid at the equivalent site of Asn-181 of $SSL4_t$, such as SSL5 and SSL2 of strain MW2, bind sLe^x in a position to form multiple hydrogen bonds to Fuc and have increased affinity for sLe^x. Those with histidine at this position and threonine at the preceding position bind sLe^x, as for SSL11, with reduced recognition of Fuc and a lower affinity.

SSL11 shows a similar affinity for the carbohydrate sLacNac (K_D = 2.43 μM), a truncated form of sLe^x lacking the terminal fucose, as for sLe^x (K_D = 2.32 μM). This is unlike $SSL4_t$, which shows a reduced affinity for sLacNac (K_D = 471.7 nM) compared with sLe^x (K_D = 87.0 nM). Like SSL11, the $SSL4_t$-N181H mutant shows similar affinities for sLacNac (K_D = 119.1 nM) and sLe^x (K_D = 90.8 nM). This indicates that a histidine at this position of the carbohydrate binding site forms a stronger bond to the O6 of NAG, independent of the presence of a Fuc residue, whereas an asparagine at this position forms a weaker bond to the O5 of NAG and the overall carbohydrate specificity is more dependent on Fuc. Together, this indicates a preference of SSL4 for glycans terminating in sLe^x, which includes Fuc.

Glycomics array data reflect variations in the fine specificity of SSL4 for other glycans. As for SSL11 (11), sLacNac is the core ligand for $SSL4_t$, but the affinity is increased in the presence of an attached Fuc residue, as in sLe^x. Whereas SSL11 displayed weak or no binding to similar glycans, such as sGal or sLac, trace binding was observed for $SSL4_t$. These observations support structural and quantitative affinity data highlighting differences between the binding sites and affinity to core glycans between these proteins. Reflected in this differential glycan preference is the finding that $SSL4_t$ and SSL11 do not compete for binding to cells. $SSL4_t$ is able to compete with itself, indicating that the majority of binding is target specific. It is apparent that the target molecules of these proteins are likely not identical. It has been suggested that variant carbohydrate sequences related to the sLe^x sequence, among others, are preferentially bound by one or the other of the selectins, resulting in subtle differences in their binding specificities (16). It appears that the same could be true for the carbohydrate-binding SSLs and might explain why *S. aureus* produces an array of homologous proteins to target sialyated glycoproteins with variations in their ligand preferences.

$SSL4_t$ has a similar leukocyte binding specificity to SSL11, binding preferentially to myeloid cells while not interacting to any significant degree with lymphocytes. Sialic acids are found on the terminating residues of many human-secreted and cell surface glycoproteins (40). While many glycoproteins express sLacNac, the core ligand for $SSL4_t$, it is known that sLe^x is expressed constitutively on granulocytes, monocytes, and a small percentage of T cells (32). This matches the leukocyte binding profile of $SSL4_t$ and supports quantitative affinity data, which indicate the target receptor(s) of SSL4 is more specific than just the core sLacNac ligand and likely includes sLe^x. In additional support of this, the $SSL4_t$-N181H mutant, which has an affinity for sLe^x similar to that of $SSL4_t$ but enhanced affinity for sLacNac, competes for cell binding with $SSL4_t$ to a level identical to that of $SSL4_t$.

We believe that SSL4 is targeting sialated glycoproteins at the surface of myeloid cells to gain entry and affect cellular function through an as yet unknown mechanism. TLR2 has been shown to be the target of SSL3, which also contains the conserved carbohydrate binding site. This binding inhibited the activation of TLR2 at the surface of human and murine neutrophils and monocytes in a partially glycan-dependent manner (5). The activation of TLR2 was also shown to be inhibited by SSL4, a function shared with no other SSL studied (5). This activity, however, was several-hundred-fold less potent than that observed for SSL3 and likely reflects the fact that SSL4 is the most homologous SSL to SSL3. MRSA252 SSL4 displayed enhanced TLR2 inhibition activity, although this allele shares greater homology with SSL3 from the same strain than it does any SSL4 allele identified in this study. At the time it was sequenced, MRSA252 was the most genetically diverse *S. aureus* strain identified (21). This suggests the SSL4 and SSL3 of MRSA252 have undergone less divergence following the duplication event from where these proteins arose than in other strains. This piece of data supports our observations that the target molecules of the glycan-binding SSLs are likely not to be identical. We believe SSL4 is targeting additional receptors on the surface of these cells.

$SSL4_t$ is actively internalized into neutrophils, macrophages, and, to a lesser extent, monocytes, in a totally glycan-dependent

manner. $SSL4_t$-R182A, which does not bind sLe^x in quantitative binding analysis, also shows a complete loss of cell binding. Identification of the target receptor(s) for SSL4 at the surface of these cells would lead to further insights into the function of this virulence factor. Interestingly, $SSL4_t$ displays different staining patterns for these cell types. While being actively internalized into discrete intracellular vesicles by neutrophils and monocytes, $SSL4_t$ staining of macrophages shows a distinct cytoskeleton-like diffuse staining. If SSL4 is targeting the cytoskeleton of macrophages, it will be interesting to determine the effects this would have on cellular mobility and intracellular functions.

Sialic acids are a convenient target for microbes, which utilize them as a scaffold for host recognition, attachment, and invasion (8). A wide variety of microbial and viral adhesins, pili, fimbriae, and hemagglutinins all target sialated glycoproteins. *S. aureus* extends this by utilizing the adaptable Sag structure to produce six homologous proteins that contain a highly conserved sialated glycan binding site. Recent studies have shown the *ssl* genes to be negatively regulated by the quorum-sensing accessory gene regulator (Agr) and to be expressed in large quantities following dysfunction in this gene regulator (6). Natural *agr*-defective strains of *S. aureus* frequently occur during infection, and these strains have been shown to have residual virulence due to overproduction of these immunomodulatory proteins (6, 38). It is interesting to speculate as to what potent effect these SSL proteins may have when expressed together to promote staphylococcal survival and persistence during colonization and infection.

ACKNOWLEDGMENTS

We thank F. Clow of the Biacore Bionsensing Facility, J. Ross of the Biomedical Imaging Research Unit, and S. Edgar of the Flow Cytometry Facility of the University of Auckland for technical support.

We acknowledge the support of the Functional Glycomics Consortium, San Diego, funded by NIH grant GM62116. This work was supported by the Maurice Wilkins Centre for Molecular Biodiscovery and grants from the Health Research Council of New Zealand.

REFERENCES

1. **Adams PD, et al.** 2002. PHENIX: building new software for automated crystallographic structure determination. Acta Crystallogr. D Biol. Crystallogr. **58**:1948–1954.
2. **Arcus VL, Langley R, Proft T, Fraser JD, Baker EN.** 2002. The three-dimensional structure of a superantigen-like protein, SET3, from a pathogenicity island of the Staphylococcus aureus genome. J. Biol. Chem. **277**: 32274–32281.
3. **Baba T, Bae T, Schneewind O, Takeuchi F, Hiramatsu K.** 2008. Genome sequence of Staphylococcus aureus strain Newman and comparative analysis of staphylococcal genomes: polymorphism and evolution of two major pathogenicity islands. J. Bacteriol. **190**:300–310.
4. **Baker HM, et al.** 2007. Crystal structures of the staphylococcal toxin SSL5 in complex with sialyl Lewis X reveal a conserved binding site that shares common features with viral and bacterial sialic acid binding proteins. J. Mol. Biol. **374**:1298–1308.
5. **Bardoel BW, et al. 20 June** 2012. Evasion of Toll-like receptor 2 activation by staphylococcal superantigen-like protein 3. J. Mol. Med. [Epub ahead of print.] doi:10.1007/s00109-012-0926-8.
6. **Benson MA, et al.** 2011. Staphylococcus aureus regulates the expression and production of the staphylococcal superantigen-like secreted proteins in a Rot-dependent manner. Mol. Microbiol. **81**:659–675.
7. **Bestebroer J, et al.** 2007. Staphylococcal superantigen-like 5 binds PSGL-1 and inhibits P-selectin-mediated neutrophil rolling. Blood **109**: 2936–2943.
8. **Bishop JR, Gagneux P.** 2007. Evolution of carbohydrate antigens—microbial forces shaping host glycomes? Glycobiology **17**:23R–34R.
9. **Bronner S, Monteil H, Prevost G.** 2004. Regulation of virulence determinants in Staphylococcus aureus: complexity and applications. FEMS Microbiol. Rev. **28**:183–200.
10. **Chenna R, et al.** 2003. Multiple sequence alignment with the Clustal series of programs. Nucleic Acids Res. **31**:3497–3500.
11. **Chung MC, et al.** 2007. The crystal structure of staphylococcal superantigen-like protein 11 in complex with sialyl Lewis X reveals the mechanism for cell binding and immune inhibition. Mol. Microbiol. **66**:1342–1355.
12. **Collaborative Computational Project No. 4.** 1994. The CCP4 suite: programs for protein crystallography. Acta Crystallogr. D Biol. Crystallogr. **50**:760–763.
13. **Daigneault M, Preston JA, Marriott HM, Whyte MKB, Dockrell DH.** 2010. The identification of markers of macrophage differentiation in PMA-stimulated THP-1 cells and monocyte-derived macrophages. PLoS One **5**:e8668. doi:10.1371/journal.pone.0008668.
14. **Davis IW, Murray LW, Richardson JS, Richardson DC.** 2004. MolProbity: structure validation and all-atom contact analysis for nucleic acids and their complexes. Nucleic Acids Res. **32**:W615–W619.
15. **Emsley P, Cowtan K.** 2004. Coot: model-building tools for molecular graphics. Acta Crystallogr. D Biol. Crystallogr. **60**:2126–2132.
16. **Feizi T.** 2000. Carbohydrate-mediated recognition systems in innate immunity. Immunol. Rev. **173**:79–88.
17. **Foster TJ.** 2005. Immune evasion by staphylococci. Nat. Rev. Microbiol. **3**:948–958.
18. **Foster TJ.** 2004. The Staphylococcus aureus "superbug." J. Clin. Invest. **114**:1693–1696.
19. **Fridkin SK, et al.** 2005. Methicillin-resistant Staphylococcus aureus disease in three communities. N. Engl. J. Med. **352**:1436–1444.
20. **Herbert S, et al.** 2007. Molecular basis of resistance to muramidase and cationic antimicrobial peptide activity of lysozyme in staphylococci. PLoS Pathog. **3**:e102. doi:10.1371/journal.ppat.0030102.
21. **Holden MTG, et al.** 2004. Complete genomes of two clinical Staphylococcus aureus strains: evidence for the evolution of virulence and drug resistance. Proc. Natl. Acad. Sci. U. S. A. **101**:9786–9791.
22. **Jongerius I, et al.** 2007. Staphylococcal complement evasion by various convertase-blocking molecules. J. Exp. Med. **204**:2461–2471.
23. **Kabsch W.** 1993. Automatic processing of rotation diffraction data from crystals of initially unknown symmetry land cell constants. J. Appl. Crystallogr. **26**:795–800.
24. **Kuroda M, et al.** 2001. Whole genome sequencing of meticillin-resistant Staphylococcus aureus. Lancet **357**:1225–1240.
25. **Langley R, Patel D, Jackson N, Clow F, Fraser JD.** 2010. Staphylococcal superantigen super-domains in immune evasion. Crit. Rev. Immunol. **30**:149–165.
26. **Langley R, et al.** 2005. The staphylococcal superantigen-like protein 7 binds IgA and complement C5 and inhibits IgA-FcαRI binding and serum killing of bacteria. J. Immunol. **174**:2926–2933.
27. **Laursen NS, et al.** 2010. Structural basis for inhibition of complement C5 by the SSL7 protein from Staphylococcus aureus. Proc. Natl. Acad. Sci. U. S. A. **107**:3681–3686.
28. **Lindsay JA, Holden MTG.** 2006. Understanding the rise of the superbug: investigation of the evolution and genomic variation of Staphylococcus aureus. Funct. Integr. Genomics **6**:186–201.
29. **Lowy FD.** 1998. Medical progress: Staphylococcus aureus infections. N. Engl. J. Med. **339**:520–532.
30. **Luong TT, Lee CY.** 2002. Overproduction of type 8 capsular polysaccharide augments Staphylococcus aureus virulence. Infect. Immun. **70**:3389–3395.
31. **Moreland N, et al.** 2005. A flexible and economical medium-throughput strategy for protein production and crystallization. Acta Crystallogr. D Biol. Crystallogr. **61**:1378–1385.
32. **Munro JM, et al.** 1992. Expression of sialyl-Lewis X, an E-selectin ligand, in inflammation, immune processes, and lymphoid tissues. Am. J. Pathol. **141**:1397–1408.
33. **Murshudov GN, Vagin AA, Dodson EJ.** 1997. Refinement of macromolecular structures by the maximum-likelihood method. Acta Crystallogr. D Biol. Crystallogr. **53**:240–255.
34. **Papageorgiou AC, Acharya KR.** 2000. Microbial superantigens: from structure to function. Trends Microbiol. **8**:369–375.
35. **Patel D, Wines BD, Langley RJ, Fraser JD.** 2010. Specificity of staphylococcal superantigen-like protein 10 toward the human IgG1 Fc domain. J. Immunol. **184**:6283–6292.
36. **Ramsland PA, et al.** 2007. Structural basis for evasion of IgA immunity by

Staphylococcus aureus revealed in the complex of SSL7 with Fc of human IgA1. Proc. Natl. Acad. Sci. U. S. A. **104**:15051–15056.
37. **Rooijakkers SHM, Van Kessel KPM, Van Strijp JAG.** 2005. Staphylococcal innate immune evasion. Trends Microbiol. **13**:596–601.
38. **Shopsin B, et al.** 2008. Prevalence of agr dysfunction among colonizing Staphylococcus aureus strains. J. Infect. Dis. **198**:1171–1174.
39. **Storoni LC, McCoy AJ, Read RJ.** 2004. Likelihood-enhanced fast rotation functions. Acta Crystallogr. D Biol. Crystallogr. **60**:432–438.
40. **Varki A.** 2007. Glycan-based interactions involving vertebrate sialic-acid-recognizing proteins. Nature **446**:1023–1029.
41. **Voyich JM, et al.** 2005. Insights into mechanisms used by Staphylococcus aureus to avoid destruction by human neutrophils. J. Immunol. **175**: 3907–3919.
42. **Wilson GJ, et al.** 2011. A novel core genome-encoded superantigen contributes to lethality of community-associated MRSA necrotizing pneumonia. PLoS Pathog. **7**:e1002271. doi:10.1371/journal.ppat.1002271.